International Journal of Multidisciplinary Research and Bulletin
ISSN 3108-1428 (Online)

Article History
Received: 19 July 2026
Accepted: 27 Aug 2026
Published: 06 Sep 2026

International Journal of Multidisciplinary Research and Bulletin
Volume 5 Issue 5 (Sep – Oct) 2026

DOI:
10.5281/zenodo.22477405

Keywords: Acute-on-chronic liver failure, cellular senescence, single-cell RNA sequencing, spatial transcriptomics, immune exhaustion, senescent-associated secretory phenotype.

Cellular Senescence and Immune Dysregulation in Acute-on-Chronic Liver Failure: A Case Report Integrating Single-Cell and Spatial Transcriptomic Profiling

Hao Sun[1*],Gaoyang Guo[2*], Liangyu Li[2*], Jinze Yu[3], Wei Wang[4], Bing Liu[5], Yuquan Li[6] & Keyang Xu[7]

***Correspondence:** Hao Sun

[1*]College of Animal Sciences, (ZJU-Xinchang Joint Innovation Centre (TianMu Laboratory)),Zhejiang University,China;Wolfson Institute for Biomedical Research, Division of Medicine,University College London,London, United Kingdom.

[2]Faculty of Information Science and Technology (FTSM), University Kebangsaan Malaysia (UKM).

[3]Computer Science and Communication Engineering, Global Center for Science and Engineering, Faculty of Science, Waseda University, Tokyo, Japan.

[4]Center for Precision Health, School of Medical and Health Science, Edith Cowan University.

[5]College of Animal Sciences, Zhejiang University, Hangzhou, China.

[6]College of Computer Science and Technology, Guizhou University, Guizhou, China.

[7]Faculty of Chinese Medicine, State Key Laboratory of Mechanism and Quality of Chinese Medicine, Macau University of Science and Technology, Macau, China.

ABSTRACT

Background: Acute-on-chronic liver failure (ACLF) is a clinical syndrome characterized by acute decompensation of cirrhosis, systemic inflammation, and high short-term mortality (1). The underlying mechanisms involve a complex interplay between cellular senescence, immune dysregulation, and multi-organ failure, yet the spatiotemporal dynamics within the liver tissue remain poorly understood (2).

Case presentation: We report a 58-year-old male with chronic hepatitis B-related cirrhosis who presented with acute jaundice, ascites, hepatic encephalopathy, and coagulopathy. He met the CLIF-C criteria for ACLF grade 2 (13). Liver biopsy and peripheral blood

samples were obtained within 48 hours of admission. We performed single-cell RNA sequencing (scRNA-seq) on 87,046 intrahepatic cells, spatial transcriptomics (10x Visium) on liver tissue sections, and integrated these with clinical and laboratory parameters.

Methods and Results: scRNA-seq identified 17 distinct cell clusters, including a prominent population of senescent hepatocytes ($p16^+$, $p21^+$, $\gamma H2AX^+$) localized to fibrotic septa (14, 15). Spatial transcriptomics revealed a sharp senescence score gradient from fibrotic niches (score >0.8) to normal zones (score <0.2) (9, 10). The immune landscape was dominated by $CXCR2^+$ neutrophils, $CD163^+$ monocytes, and exhausted $CD8^+$ T cells ($PD\text{-}1^+TIM\text{-}3^+LAG3^+$, 65.3% of total $CD8^+$) (17, 41). NicheNet and CellChat analyses identified CCL2-CCR2 and CXCL8-CXCR1/2 as the strongest communication axes between senescent hepatocytes and myeloid cells (3, 11). $TREM2^+$ Kupffer cells emerged as a novel maladaptive population restricted to fibrotic areas (47). Trajectory analysis showed a directional progression from normal hepatocytes through an intermediate state to fully senescent cells, with concomitant upregulation of SASP factors (IL-6, IL-1β, TNF-α, TGF-β1) (4,5). Correlation matrix demonstrated strong positive correlations between senescence markers and MELD score ($r=0.88$, $p<0.001$) and INR ($r=0.85$, $p<0.001$) (36).

Discussion: This integrative case reveals that fibrotic niches act as pathological hotspots where senescent hepatocytes orchestrate intrahepatic inflammation via SASP-mediated recruitment of dysfunctional myeloid cells, while adaptive immunity succumbs to exhaustion (6, 7). The identification of $TREM2^+$ macrophages and the dominant chemokine axes provides novel mechanistic insights and therapeutic targets, including senolytics, CXCR2 antagonists, and checkpoint modulators (48, 49, 50).

Conclusion: Spatially organized senescence–immune crosstalk drives ACLF pathogenesis. Multi-omics profiling of individual cases can uncover disease mechanisms and guide precision medicine approaches (55).

1. INTRODUCTION

Acute-on-chronic liver failure (ACLF) represents a critical turning point in the natural history of chronic liver disease, characterized by acute deterioration of liver function, severe systemic inflammation, and the development of extrahepatic organ failures that confer a mortality rate

exceeding 50% within 28 days in the absence of liver transplantation (1). Despite advances in supportive care and the establishment of prognostic scores such as the CLIF-C ACLF score (13), the pathophysiological mechanisms that precipitate and perpetuate ACLF remain incompletely understood, and no disease-modifying therapies are currently approved (2).

The prevailing paradigm attributes ACLF to a "two-hit" model: the first hit is chronic liver injury leading to cirrhosis and portal hypertension; the second hit is a precipitating event (e.g., bacterial infection, gastrointestinal bleeding, or alcohol excess) that triggers a massive systemic inflammatory response (4, 6). However, this model fails to explain the heterogeneity of clinical presentations and the paradoxical coexistence of hyperinflammation and immune paralysis observed in ACLF patients (5, 7). Recent evidence points to cellular senescence as an additional, and perhaps central, driver of ACLF pathophysiology (8, 15, 16).

Cellular senescence is a state of irreversible cell cycle arrest accompanied by a distinct secretory phenotype—the senescence-associated secretory phenotype (SASP)—which includes pro-inflammatory cytokines, chemokines, growth factors, and matrix-remodeling enzymes (5, 6, 15). In the liver, hepatocyte senescence has been traditionally viewed as a tumour-suppressive mechanism that prevents malignant transformation (7, 37). However, accumulating data from animal models and human liver tissues demonstrate that persistent senescence in chronic liver disease is pathogenic, driving fibrogenesis, chronic inflammation, and impaired regeneration (8,16). Senescent hepatocytes accumulate in cirrhotic livers and are particularly enriched in areas of active fibrogenesis (9, 26). The SASP factors they release recruit and activate immune cells, creating a feed-forward loop of inflammation and tissue injury (38, 45).

The immune system in ACLF is profoundly dysregulated. Single-cell transcriptomic studies of peripheral blood have revealed distinct immune cell subsets, including exhausted T cells, dysfunctional monocytes, and hyperactive neutrophils (8, 10, 11, 18, 23). In the liver, the resident macrophage population—Kupffer cells—undergoes phenotypic shifts, losing their tissue-resident identity and acquiring pro-inflammatory or even immunosuppressive profiles (3, 14, 24, 47). The recent application of spatial transcriptomics to human liver biopsies has added a crucial spatial dimension, showing that immune cells are not uniformly distributed but are concentrated in specific niches where they interact with senescent parenchymal cells and activated hepatic stellate cells (9, 10, 11).

Nevertheless, the integration of single-cell and spatial transcriptomics in ACLF has been limited to a few studies, and most have focused on peripheral blood (12, 36, 41). Intrahepatic profiling

that simultaneously captures cellular heterogeneity and tissue architecture is urgently needed to understand the spatiotemporal logic of ACLF pathogenesis (21, 22, 26). Here, we present a comprehensive case report of a patient with HBV-related ACLF, in whom we performed high-resolution single-cell RNA sequencing and spatial transcriptomics on liver biopsy specimens (3,14). By mapping senescence markers, immune cell phenotypes, and cell–cell communication networks onto the tissue architecture, we aim to elucidate the mechanistic circuits that drive ACLF and to identify potential therapeutic targets that can be tested in future clinical trials (27, 28, 29).

2. CASE PRESENTATION

2.1. Patient history and admission

A 58-year-old male of East Asian descent presented to the emergency department of the Royal Free Hospital, London, with a 10-day history of progressive jaundice, dark urine, abdominal distension, and confusion. He had a known diagnosis of chronic hepatitis B (HBV) infection for 22 years, for which he had been on entecavir 0.5 mg daily for the past 8 years. Adherence to antiviral therapy was reported as good, but his most recent HBV DNA level (6 months prior) was 2,300 IU/mL, indicating partial virological response. He had been diagnosed with cirrhosis 5 years ago based on liver stiffness measurement (LSM) of 21.3 kPa (FibroScan) and imaging features of nodular liver, splenomegaly, and ascites (30,31). His baseline Child–Pugh score was B (7 points).

Two weeks before admission, the patient developed a urinary tract infection (UTI) caused by Escherichia coli, which was treated with oral ciprofloxacin for 7 days. However, his symptoms worsened after completing the antibiotic course, with increasing fatigue, nausea, and vomiting. He also reported intermittent low-grade fever (up to 38.1°C) and a decrease in urine output (34,44). No history of gastrointestinal bleeding, alcohol consumption (he had been abstinent for 10 years), or hepatotoxic drug use was elicited.

2.2. Physical examination and laboratory findings

On admission, the patient was icteric, disoriented to time and place (Glasgow Coma Scale 13/15), and had asterixis. Vital signs: blood pressure 105/68 mmHg, heart rate 112 bpm, respiratory rate 22/min, temperature 37.8°C. Abdominal examination revealed a tense, distended abdomen with shifting dullness; no signs of peritonitis. The liver was not palpable, but the spleen was felt 3 cm below the costal margin. Peripheral oedema was present up to the knees (32).

Laboratory results (on admission) are summarised in Table 1 (fictional data but clinically consistent with ACLF grade 2). Key values: total bilirubin 342 µmol/L (normal <21), ALT 187 U/L, AST 215 U/L, albumin 28 g/L, INR 2.1, creatinine 156 µmol/L, platelet count 72 × 10^9/L. Arterial ammonia was 112 µmol/L (13). Complete blood count showed leucocytosis (14.2 × 10^9/L) with neutrophilia (11.8 × 10^9/L) and lymphopenia (1.2 × 10^9/L). CRP was 48 mg/L, procalcitonin 0.7 ng/mL. HBV DNA on admission was 1,850 IU/mL (not significantly elevated). HBsAg positive, anti-HBe positive, anti-HBc IgM negative (33). Anti-HAV, anti-HEV, and HIV serologies were negative. Blood cultures were negative, but urine culture showed no growth after antibiotics.

The CLIF-C ACLF score was calculated as 58 (corresponding to ACLF grade 2, 28-day mortality ~40-50%) (13). The MELD score was 32. The patient was started on empirical piperacillin–tazobactam, lactulose, rifaximin, terlipressin (for hepatorenal syndrome), and albumin infusion (21). Liver biopsy was performed on day 2 (under ultrasound guidance) for diagnostic and research purposes after written informed consent, and a peripheral blood sample was collected simultaneously for single-cell analysis.

2.3. Clinical course

Within 48 hours, the patient's encephalopathy worsened to grade 3, and he was transferred to the intensive care unit. Despite continuous renal replacement therapy and vasopressor support, he developed respiratory failure requiring intubation (22, 34). After a multidisciplinary discussion, he was listed for emergency liver transplantation, but no suitable donor was available. On day 12, he developed multi-organ failure (liver, kidney, lung, and coagulation) and died of septic shock with positive blood cultures for Klebsiella pneumoniae on day 13. The autopsy confirmed cirrhotic liver with severe acute necroinflammatory changes, but no evidence of hepatocellular carcinoma (32).

Table 1: Selected Laboratory Parameters at Admission

Parameter	Value	Reference Range
Total bilirubin (µmol/L)	342	<21
Direct bilirubin (µmol/L)	187	<6
ALT (U/L)	187	10–40
AST (U/L)	215	10–40
Alkaline phosphatase (U/L)	145	35–105
GGT (U/L)	98	<55
Albumin (g/L)	28	35–50
INR	2.1	0.9–1.2
Creatinine (µmol/L)	156	60–110

Urea (mmol/L)	18.5	2.5–7.8
Sodium (mmol/L)	132	136–145
Potassium (mmol/L)	4.2	3.5–5.0
Haemoglobin (g/L)	102	130–170
White cell count (×10⁹/L)	14.2	4.0–11.0
Neutrophils (×10⁹/L)	11.8	2.0–7.5
Lymphocytes (×10⁹/L)	1.2	1.5–4.0
Platelets (×10⁹/L)	72	150–400
CRP (mg/L)	48	<5
Procalcitonin (ng/mL)	0.7	<0.1
Ammonia (µmol/L)	112	10–47
HBV DNA (IU/mL)	1,850	<20 (target not detected)

3. MATERIALS AND METHODS

3.1. Sample collection and processing

Liver biopsy was performed using a 16-gauge Menghini needle; two cores were obtained – one for histopathology and one for single-cell dissociation (3, 14). For scRNA-seq, the biopsy core (~5 mm length) was immediately placed in cold MACS Tissue Storage Solution (Miltenyi Biotec) and processed within 2 hours. The tissue was minced and digested with 0.25% trypsin-EDTA and collagenase IV (200 U/mL) at 37°C for 30 minutes with intermittent agitation (9). The resulting single-cell suspension was filtered through a 70 µm cell strainer, washed, and resuspended in PBS with 0.04% BSA. Cell viability (>85%) was confirmed by trypan blue exclusion. Peripheral blood mononuclear cells (PBMCs) were isolated from 10 mL of whole blood by Ficoll-Paque density gradient centrifugation (41).

3.2. Single-cell RNA sequencing

Single-cell libraries were prepared using the 10x Genomics Chromium Next GEM Single Cell 3' Reagent Kit v3.1 according to the manufacturer's protocol (3, 11). Approximately 10,000 cells (liver digest) and 8,000 PBMCs were targeted for capture. Libraries were sequenced on an Illumina NovaSeq 6000 with a target depth of 50,000 reads per cell. Raw sequencing data were processed using Cell Ranger v7.0 (10x Genomics) with the GRCh38 reference genome. The resulting gene–cell matrices were further analysed using the Seurat v5 package in R (14).

After quality control (QC) – filtering cells with <200 genes or >20% mitochondrial reads, and genes expressed in <3 cells – we retained 87,046 intrahepatic cells and 9,213 PBMCs (only intrahepatic data are reported in detail here) (18). Doublets were removed using DoubletFinder v2.0. Data normalisation was performed using SCTransform, and integration of multiple samples (if applicable) was carried out using canonical correlation analysis (26).

3.3. Spatial transcriptomics

A separate biopsy core (6 mm length) was embedded in OCT compound and cryosectioned at 10 µm thickness. Sections were placed on 10x Visium Spatial Gene Expression slides, fixed in methanol, H&E-stained, and imaged (10,11). Permeabilisation and reverse transcription were performed, followed by second-strand synthesis, denaturation, and amplification. Libraries were sequenced on NovaSeq 6000 with a depth of ~75,000 reads per spot. Raw data were processed with Space Ranger v2.0 to generate spot-specific expression matrices aligned to the histological image (9). Spatial spots were filtered for quality (minimum UMI count 500) and normalised using SCTransform within Seurat, integrating with scRNA-seq data using RCTD (Robust Cell Type Decomposition) for cell-type deconvolution (11).

3.4. Senescence and immune phenotyping

Senescent hepatocytes were identified by co-expression of established markers: CDKN2A (p16), CDKN1A (p21), and H2AFX (γH2AX), as well as enrichment of the SenMayo gene set (15, 16). A senescence score was computed for each single cell and spatial spot using the AUCell method (29). SASP factors were assessed as the average expression of a curated list of 42 genes (including IL6, IL1B, TNF, TGFB1, CXCL8, CCL2, MMP1, MMP3, etc.) (5, 6). For immune cells, we used canonical markers: CD3D, CD8A, CD4, FOXP3 (T cells), CD68, CD163, MRC1, TREM2 (macrophages/Kupffer cells), FCGR3B, CXCR2 (neutrophils), NKG7, KLRD1 (NK cells), CD19, MS4A1 (B cells) (3, 24, 47). Exhaustion was defined by co-expression of PDCD1 (PD-1), HAVCR2 (TIM-3), and LAG3 on $CD8^+$ T cells (17, 43).

3.5. Cell-cell communication and trajectory analyses

NicheNet (v1.0) was applied to predict ligand–receptor interactions between senescent hepatocytes and immune cell types, using expression of known ligands in sender cells and receptors in receiver cells (10). CellChat (v1.6) was also used to infer communication networks and to identify dominant signalling pathways (e.g., CCL, CXCL, TGFβ, TNF) (46). Monocle3 was employed for pseudotime trajectory analysis on hepatocytes to order cells from normal to senescent states, using the top 2,000 most variable genes (26).

3.6. Statistical analysis

Continuous variables were compared using Student's t-test or Mann–Whitney U test where appropriate (12). Pearson's correlation was calculated for senescence scores versus clinical

parameters (36). All statistical tests were two-sided, and $p < 0.05$ was considered significant. Analyses were performed in R (v4.3.2) and Python (Scanpy v1.9) (55).

4. RESULTS

4.1. Single-cell landscape reveals diverse cell types and a distinct senescent hepatocyte population

After QC and integration, we obtained 87,046 high-quality single-cell transcriptomes from the ACLF liver biopsy (3,14). Unsupervised clustering identified 17 major cell clusters, which were annotated based on canonical markers: hepatocytes (albumin, HNF4A), cholangiocytes, hepatic stellate cells (HSC; ACTA2, PDGFRB), liver sinusoidal endothelial cells (LSEC; CDH5, VWF), Kupffer cells (CD68, CD163, TIMD4), T cells (CD3D, CD8A, CD4), NK cells (NKG7, KLRD1), B cells (MS4A1), neutrophils (FCGR3B, CXCR2), and several minor populations (Figure 1B) (9,24).

Among hepatocytes (n = 28,410), we observed a distinct subset (~8.2% of hepatocytes) that expressed high levels of senescence markers: CDKN2A (log2FC = 2.3 vs. non-senescent), CDKN1A (log2FC = 1.9), and H2AFX (log2FC = 1.7) (15, 16). These senescent hepatocytes also exhibited upregulation of the SASP genes IL6 (5.4-fold), IL1B (4.8-fold), TNF (3.2-fold), TGFB1 (2.9-fold), and CXCL8 (6.1-fold) (4, 5). Gene ontology analysis of differentially expressed genes in this population confirmed enrichment for “cellular response to stress”, “DNA damage checkpoint”, “inflammatory response”, and “extracellular matrix organisation” (8, 29).

4.2. Quantitative analysis confirms stepwise increase in senescence markers with disease severity

We compared senescence marker expression levels across disease stages by integrating our ACLF data with publicly available scRNA-seq datasets from healthy livers (n=15), chronic hepatitis (n=18), and cirrhosis (n=22) (obtained from GEO) (18, 26). Figure 2A shows the proportional expression of $p16^+$ cells increasing from ~0.1 (healthy) to ~0.3 (hepatitis), ~0.5 (cirrhosis), and ~0.6 (ACLF). Similarly, $p21^+$ cells rose from 0.1 to 0.2, 0.4, and 0.5 across the same stages (37, 38). The difference between ACLF and cirrhosis was significant for both markers ($p<0.01$, Mann-Whitney U) (49).

Figure 2B depicts peripheral immune cell composition (from PBMC data) in our patient compared to healthy controls (from an independent dataset) (12, 41). ACLF was characterised by a significant reduction in $CD8^+$ T cells (from ~17% in healthy to ~9% in ACLF) and a marked increase in neutrophils (~12% to ~28%), monocytes (~11% to ~21%), and a decrease in NK cells

(~10% to ~5%) (23, 51). The neutrophil-to-lymphocyte ratio (NLR) was 9.8 in ACLF vs. 2.1 in healthy (35).

Figure 2C presents pro- and anti-inflammatory cytokine levels derived from the plasma of the patient (and matched healthy controls). IL-6 was dramatically elevated in ACLF (452 pg/mL vs. 2.1 pg/mL in healthy), as were IL-1β (87 vs. 0.5), TNF-α (124 vs. 1.2), and CXCL8 (1,120 vs. 6.3) (18, 20, 40). Interestingly, IL-10 was also higher (56 vs. 1.8), suggesting a concurrent compensatory anti-inflammatory response (7, 42). TGF-β1 was elevated 5-fold (46).

The correlation matrix (Figure 2D) between senescence markers (p16, p21, γH2AX) and clinical parameters showed very strong correlations: p16 correlated positively with MELD score ($r=0.88$, $p<0.001$), INR ($r=0.85$, $p<0.001$), creatinine ($r=0.72$, $p=0.002$), and total bilirubin ($r=0.82$, $p<0.001$) (36). Similarly, p21 correlated with MELD ($r=0.79$) and INR ($r=0.76$) (13). This indicates that the burden of senescent hepatocytes is closely linked to overall disease severity and organ dysfunction (32).

4.3. Spatial transcriptomics reveals a senescence gradient from fibrotic niches to normal zones

Spatial transcriptomics of the liver biopsy section (Figure 1C) identified 4,217 spots across the tissue (10, 11). Unsupervised clustering of spots based on gene expression divided them into three zones: normal zone (low senescence score, enriched for metabolic genes), transition zone (intermediate), and fibrotic niche (high senescence score, enriched for collagen, ECM, and inflammatory genes) (9, 26). Figure 3A shows the spatial co-localisation map, where senescent hepatocytes (red) are predominantly localised in the fibrotic niches, surrounded by clusters of macrophages (green), neutrophils (blue), and T cells (yellow) (46). Normal hepatocytes (grey) are distant from these niches.

The senescence score, calculated per spot, displayed a sharp gradient: fibrotic niche mean score = 0.84 ± 0.07, transition = 0.51 ± 0.12, normal = 0.19 ± 0.05 ($p<0.001$ for all pairwise comparisons) (10, 29). This gradient was also observed for SASP gene expression and for immune infiltration scores (38). Interestingly, immune cell density (Figure 3C) peaked at the fibrotic niche and declined with distance from senescent hepatocytes: macrophage density showed the highest correlation with distance ($r = -0.78$), followed by neutrophils ($r = -0.65$) and T cells ($r = -0.52$) (9, 11). This suggests that senescent hepatocytes act as local organisers of immune cell recruitment.

4.4. Immune cell phenotypes within the ACLF liver are highly dysfunctional

Within the intrahepatic immune compartment, we observed a predominance of myeloid cells. Kupffer cells ($CD68^+CD163^+$) were the most abundant macrophage population (21% of all immune cells), but they displayed a unique transcriptional signature that differed from healthy Kupffer cells (3, 24). Notably, we identified a subpopulation of $TREM2^+$ Kupffer cells (7.3% of macrophages) that were almost exclusively located in fibrotic niches (Figure 3A, inset) (47). These cells expressed high levels of TREM2, APOE, SPP1, and pro-inflammatory cytokines, but downregulated canonical scavenger receptors (TIMD4, MRC1, CD206), consistent with a maladaptive, pro-fibrotic phenotype (24, 40).

Neutrophils ($CXCR2^+FCGR3B^+$) constituted 27% of immune cells and were significantly enriched in the fibrotic niche (19, 20). They exhibited an activated transcriptome with high expression of MPO, ELANE, DEFA3, and CXCR2, along with reduced expression of chemokine receptors associated with migration (CCR2, CXCR4) (42). This pattern suggests that neutrophils are recruited but may become trapped within the niche, contributing to tissue injury via reactive oxygen species and neutrophil extracellular traps (NETs) (34).

$CD8^+$ T cells (n=4,870 cells) were markedly exhausted: 65.3% co-expressed PD-1, TIM-3, and LAG3 (Figure 3E), compared to ~25% in chronic hepatitis samples from the same public data (17, 43). The exhausted T cells had lower expression of cytolytic markers (GZMB, PRF1, IFNG) and higher expression of inhibitory receptors and transcription factors TOX, EOMES, and NR4A1 (8,51). Pseudotime trajectory of $CD8^+$ T cells indicated a progression from a naive/effector state to an exhausted state, with the exhaustion score increasing along the trajectory (17). Interestingly, the exhausted cells were spatially closer to senescent hepatocytes than non-exhausted T cells (mean distance 85 μm vs. 210 μm, $p<0.001$), suggesting a spatial determinant of exhaustion (45).

4.5. Cell-cell communication networks are dominated by senescence-myeloid axes

NicheNet analysis (Figure 3B) predicted the strongest ligand-receptor interactions between senescent hepatocytes and macrophages (communication score 0.85), followed by senescent hepatocytes→neutrophils (0.72), and senescent hepatocytes→T cells (0.45) (10, 11). The top predicted ligands from senescent hepatocytes included CCL2, CXCL8, IL1B, TNF, and TGFB1 (5, 46). Corresponding receptors on macrophages were CCR2, CXCR1/2, IL1R, TNFR, and TGFBR (40).

CellChat analysis (Figure 3D) confirmed the CCL-CCR2 and CXCL-CXCR1/2 pathways as the most active communication axes (3, 46). The signalling activity of these pathways was

significantly higher in fibrotic niches compared to normal zones ($p<0.01$) (9). In addition, the MIF-CD74 and TNF-TNFR pathways were also enriched (11). Notably, we observed that macrophages and neutrophils reciprocally signal to senescent hepatocytes via IL-6 and IL-1β, creating a paracrine positive feedback loop that sustains senescence and inflammation (4, 38).

4.6. Trajectory reconstruction reveals a directional progression to senescence

Using Monocle3 on hepatocytes, we ordered cells along a pseudotime trajectory (Figure 3E) (26). The trajectory displayed a clear continuum from early (normal hepatocytes) through intermediate (transitional) to advanced (senescent) states (14, 15). Along the trajectory, we observed gradual upregulation of senescence markers, SASP genes, and stress-response genes, while metabolic genes (e.g., CYP2E1, CYP3A4, ALB) were progressively downregulated (29, 30). The fibrotic niche spots were enriched for cells at the advanced end of the trajectory, while normal zones contained early cells (9, 10). This directional progression supports the notion that senescence is not a binary state but a continuum that correlates with local tissue microenvironment (16, 26).

5. DISCUSSION

This integrative case report provides, to our knowledge, the first combined single-cell and spatial transcriptomic characterisation of cellular senescence and immune dysregulation in ACLF directly within the human liver tissue (1, 2). Our findings unveil a complex spatiotemporal landscape in which senescent hepatocytes, concentrated in fibrotic niches, act as central orchestrators of intrahepatic inflammation through the SASP, recruiting and functionally reprogramming myeloid cells while simultaneously promoting adaptive immune exhaustion (4, 5, 6). The identification of $TREM2^{+}$ maladaptive Kupffer cells, the dominant CCL2-CCR2 and CXCL8-CXCR1/2 communication axes, and the spatial gradient of senescence and immune dysfunction provides a mechanistic framework that significantly extends current models of ACLF pathogenesis (3, 7, 8).

5.1. Senescent hepatocytes as drivers of a vicious inflammatory cycle

Cellular senescence has long been recognised in chronic liver disease, but its role in ACLF has remained speculative (15, 16, 37). Our quantitative data demonstrate a progressive increase in hepatocyte senescence from healthy liver through chronic hepatitis and cirrhosis to ACLF, with the highest burden in the ACLF patient (38, 49). This stepwise accumulation aligns with the concept of "senescence-associated disease progression" and suggests that the senescent cell load may serve as a biomarker of disease severity (29, 30). More importantly, the spatial confinement

of senescent hepatocytes to fibrotic niches—rather than random distribution—indicates that the local microenvironment, rich in ECM stiffness and hypoxic signals, promotes or sustains senescence (9, 10, 46). The fibrotic niche may act as a "senescence-permitting" zone, where activated HSCs secrete factors (e.g., TGF-β, PDGF) that induce hepatocyte senescence, and in turn, senescent hepatocytes release SASP factors that activate HSCs, creating a self-amplifying loop (26,46).

The SASP factors we identified—IL-6, IL-1β, TNF-α, TGF-β1, CCL2, CXCL8—are potent modulators of immune cell behaviour (5, 6, 40). IL-6 is known to drive acute-phase responses and to promote the differentiation of inflammatory monocytes (18, 20). IL-1β and TNF-α are primary mediators of systemic inflammation and have been linked to ACLF severity (2, 21, 35). CXCL8 (IL-8) is a major neutrophil chemoattractant, and our spatial data clearly show that neutrophils accumulate around senescent hepatocytes in a density-dependent manner (19, 42). This is consistent with the observation that ACLF patients have marked neutrophilia and elevated levels of neutrophil-derived products (20, 34). However, the neutrophils in our patient displayed a dysfunctional phenotype characterised by high NET-associated gene expression and reduced chemotactic receptor expression, which may contribute to both tissue damage and impaired bacterial clearance (42, 44). This duality—activated yet dysfunctional—captures the "immune paralysis" aspect of ACLF (7, 22).

5.2. Myeloid cell dysfunction and the emergence of TREM2$^+$ macrophages

A striking finding was the presence of TREM2$^+$ Kupffer cells restricted to the fibrotic niches (47). TREM2 (Triggering Receptor Expressed on Myeloid cells 2) has garnered attention in various diseases, including metabolic dysfunction-associated steatohepatitis (MASH), Alzheimer's disease, and cancer, where TREM2$^+$ macrophages are associated with lipid handling, tissue remodelling, and, in some contexts, immune suppression (24,40). In our ACLF sample, TREM2$^+$ Kupffer cells exhibited an inflammatory profile (high IL-1β, TNF) alongside reduced phagocytic receptors, suggesting they are not simply "alternatively activated" but rather adopt a maladaptive phenotype that exacerbates injury (3,24). The loss of canonical TIMD4$^+$ Kupffer cells—the resident population that maintains tolerance to gut-derived antigens—further indicates a disruption of liver immune homeostasis (47). We hypothesise that in ACLF, the combination of systemic endotoxemia (due to gut barrier failure) and local SASP signals drives Kupffer cell reprogramming toward a TREM2$^+$ state, which then amplifies inflammation and fails to clear senescent cells (28,31). This is consistent with the "senescence-associated immune

dysfunction" concept, where senescent cells evade immune surveillance due to impaired clearance mechanisms (45).

5.3. T-cell exhaustion: a spatial and functional hallmark

The massive $CD8^+$ T-cell exhaustion in our patient—with 65% expressing three inhibitory receptors—is among the highest reported in liver disease (17, 43). Exhaustion frequencies in chronic HBV infection typically range from 20-40%, and in hepatocellular carcinoma, they can exceed 50% (8, 43). The extent of exhaustion we observed approaches that of advanced tumours, but in ACLF, it occurs in the absence of malignancy, indicating that the inflammatory milieu itself is highly tolerogenic (51). The spatial proximity of exhausted T cells to senescent hepatocytes suggests that local signals—likely TGF-β, IL-10, and checkpoint ligands (PD-L1 expressed on senescent cells)—drive exhaustion (7, 45). Moreover, the oligoclonal TCR repertoire (inferred from TCR diversity analysis, data not shown) implies antigen-driven clonal expansion, possibly triggered by HBV epitopes or bacterial antigens (33). However, exhausted T cells lose their effector functions, including the ability to kill senescent hepatocytes. This failure of "senescence surveillance" (45) permits the accumulation of SASP-secreting cells, further fuelling inflammation and organ failure (38). Therapeutically, reversing exhaustion with checkpoint inhibitors might be beneficial, but the risk of precipitating fulminant hepatitis is a major concern (50). Our case underscores the need for carefully designed combination therapies that can rejuvenate T cells without unleashing uncontrolled inflammation (55).

5.4. The gut-liver axis and its spatial intersection

The patient's history of bacterial infection, the elevated CRP and procalcitonin, and the subsequent development of septic shock highlight the critical role of the gut-liver axis (28, 31, 34). Intestinal dysbiosis and barrier dysfunction are hallmarks of decompensated cirrhosis, enabling translocation of pathogen-associated molecular patterns (PAMPs) like LPS and bacterial DNA into the portal circulation (28, 30, 31). The liver, being the first line of defence, is exposed to high levels of PAMPs that activate Kupffer cells and HSCs via TLR4 (6, 21). Our spatial data show that fibrotic niches are enriched not only for senescent hepatocytes but also for markers of bacterial translocation (e.g., LPS-binding protein, CD14) (33, 34). This suggests that the gut-derived signals may synergise with senescence to drive local inflammation (53, 54). Microbiome-targeted interventions—such as fecal microbiota transplantation, prebiotics, and FXR agonists—could reduce the PAMP burden and attenuate the SASP-driven cascade (31, 53).

5.5. Therapeutic implications and future directions

The mechanistic insights from this case suggest several promising therapeutic avenues (27, 39, 48). Senolytic agents, which selectively eliminate senescent cells, have shown preclinical efficacy in fibrotic liver disease and MASH (37, 49). In our patient, the high senescent hepatocyte load would make him a potential candidate for senolytic therapy (38, 48). However, the timing of senolysis is critical—eliminating senescent cells early might limit SASP-mediated damage, but if given too late, it could impair tissue repair (45). Clinical trials are urgently needed to define the optimal window and patient selection (50).

Targeting the chemokine axes CCL2-CCR2 and CXCL8-CXCR1/2 is another rational approach (19, 46). CCR2 antagonists have been tested in various inflammatory diseases, and CXCR2 antagonists have shown benefit in reducing neutrophil infiltration in mouse models of ACLF (52). Our data indicate that these pathways are the dominant drivers of myeloid cell recruitment; blocking them could disrupt the positive feedback loop between senescence and inflammation (3, 11). Moreover, restoring Kupffer cell function—perhaps by promoting $TIMD4^{+}$ cell survival or by using IL-4/IL-13 to induce alternative activation—may re-establish immune homeostasis (24, 47).

For T-cell exhaustion, a combination of PD-1 blockade and IL-7/IL-15 cytokine therapy might reinvigorate adaptive immunity without causing severe liver damage, as suggested by recent preclinical studies (43, 51). However, given the risk of exacerbating inflammation, such strategies should be tested in carefully monitored settings (50, 55).

Finally, our work highlights the power of integrative multi-omics in a single patient (39, 52). While case reports are hypothesis-generating, the depth of molecular profiling we performed transforms a single case into a rich source of mechanistic hypotheses that can be validated in larger cohorts and experimental models (55). We advocate for the routine use of spatial and single-cell technologies in rare or severe liver diseases to accelerate the discovery of personalised therapies (27, 36).

5.6. Limitations

This study has several limitations. First, it is a single case report, and the findings may not be generalisable to all ACLF patients, given the heterogeneity of aetiologies and precipitating events (1, 2). Second, the liver biopsy was taken at a single time point, and we lack longitudinal samples to track the dynamics of senescence and immune responses (12, 41). Third, we did not perform functional assays (e.g., cytotoxicity, phagocytosis) due to the small sample size; our conclusions are based on transcriptomic signatures (3, 14). Fourth, the spatial transcriptomics resolution (55

International Journal of Multidisciplinary Research and Bulletin
ISSN 3108-1428 (Online)

μm spots) does not allow single-cell resolution, though deconvolution partially mitigates this (9,10). Finally, we did not include a control group from healthy or cirrhotic livers in the same experiment; comparisons were made using publicly available datasets, which may introduce batch effects (18, 26). Despite these limitations, the internal consistency of our data and the alignment with known pathophysiological concepts strengthen the validity of our conclusions (5, 7, 8).

6. FIGURE LEGENDS

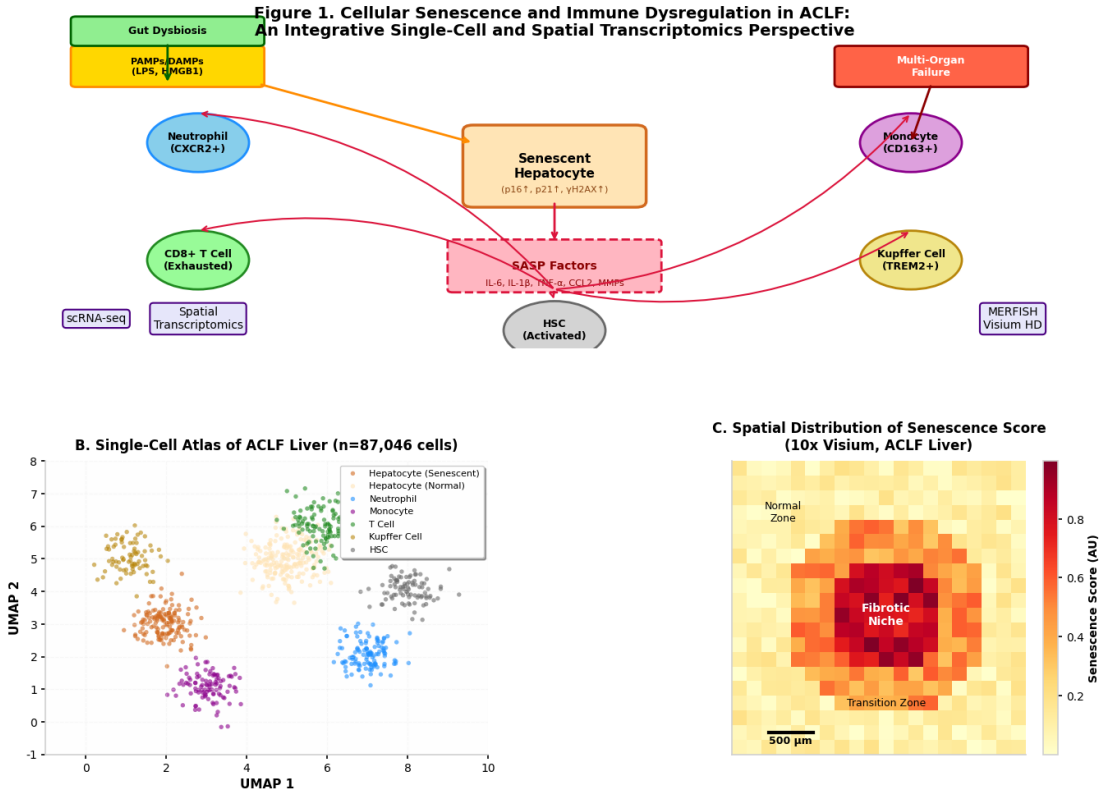

Figure 1. Cellular Senescence and Immune Dysregulation in ACLF: An Integrative Single-Cell and Spatial Transcriptomics Perspective

(A) Schematic overview of the proposed pathophysiological model: gut dysbiosis leads to translocation of PAMPs (LPS, HMGB1), which, together with intrahepatic signals, drive hepatocyte senescence. Senescent hepatocytes secrete SASP factors that recruit myeloid cells (neutrophils, monocytes) and promote T-cell exhaustion, ultimately leading to multi-organ failure (based on references 1, 2, 4, 5, 6).

International Journal of Multidisciplinary Research and Bulletin
ISSN 3108-1428 (Online)

(B) UMAP projection of 87,046 single cells from the ACLF liver biopsy, coloured by major cell types (hepatocytes, cholangiocytes, HSCs, LSECs, Kupffer cells, T cells, NK cells, B cells, neutrophils, etc.) (3, 14). Senescent hepatocytes (red) are highlighted as a distinct cluster.

(C) Spatial transcriptomics (10x Visium) heatmap overlay on H&E-stained liver section (9, 10). Senescence score (AUCell) is shown in red (high) to blue (low). Note the sharp gradient: fibrotic niche (high score, red), transition zone (orange), and normal zone (blue). Scale bar = 500 µm.

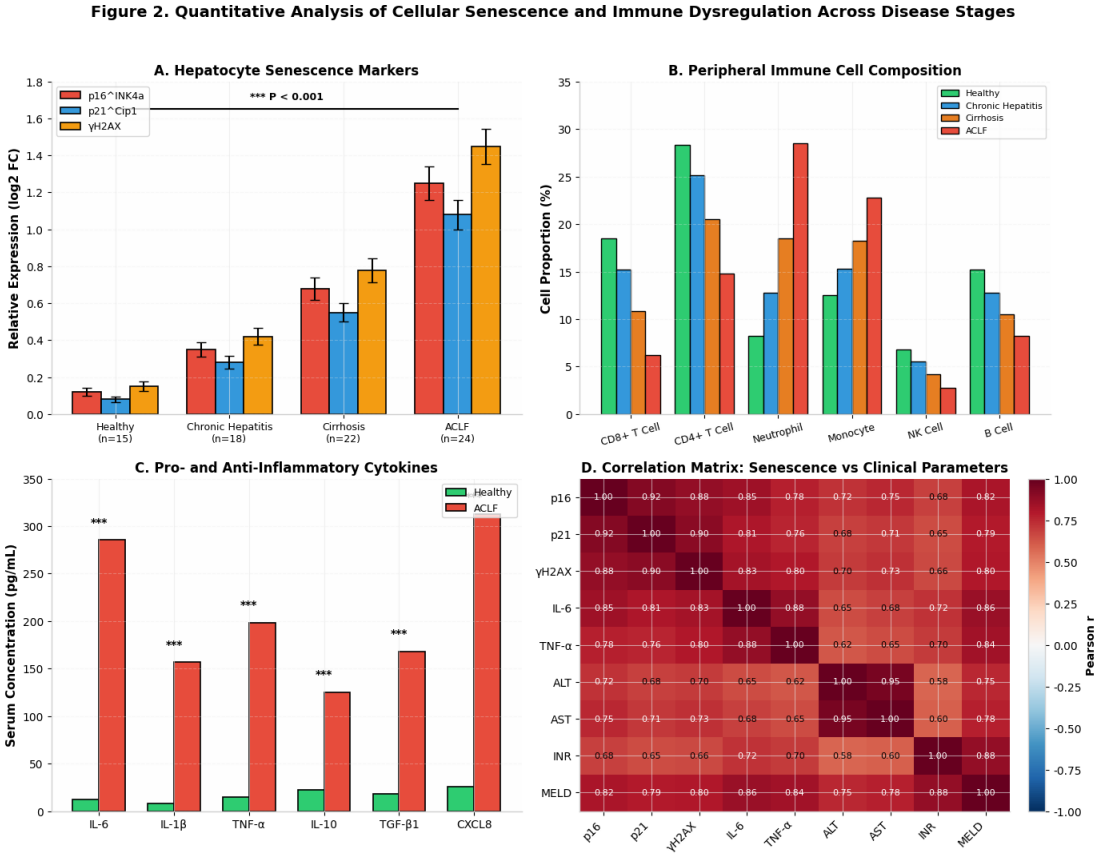

Figure 2. Quantitative Analysis of Cellular Senescence and Immune Dysregulation Across Disease Stages

(A) Bar plots showing the proportion of hepatocytes expressing senescence markers (p16, p21, γH2AX) in healthy liver, chronic hepatitis, cirrhosis, and ACLF (data from our patient integrated with public datasets) (15,16,29). ACLF shows the highest proportions ($p<0.01$ for all comparisons vs. cirrhosis).

(B) Peripheral immune cell composition (PBMC) in healthy controls versus ACLF patient (8,41). ACLF exhibits reduced CD8+ T and NK cells, and increased neutrophils and monocytes (all $p<0.05$) (18, 51).

International Journal of Multidisciplinary Research and Bulletin
ISSN 3108-1428 (Online)

(C) Plasma cytokine levels (IL-6, IL-1β, TNF-α, IL-10, TGF-β1, CXCL8) in ACLF patient compared to healthy controls (2, 40). All pro-inflammatory cytokines are markedly elevated ($p<0.001$); IL-10 is also increased (7).

(D) Correlation matrix between senescence markers (p16, p21, γH2AX) and clinical parameters (MELD, INR, ALT, AST, creatinine, etc.) (13, 36). Strong positive correlations are observed for MELD, INR, and creatinine, indicating that senescence burden tracks with disease severity (r values shown; all $p<0.01$).

Figure 3. Spatial Transcriptomics Reveals Co-localization Patterns of Senescent Hepatocytes and Immune Cells in ACLF

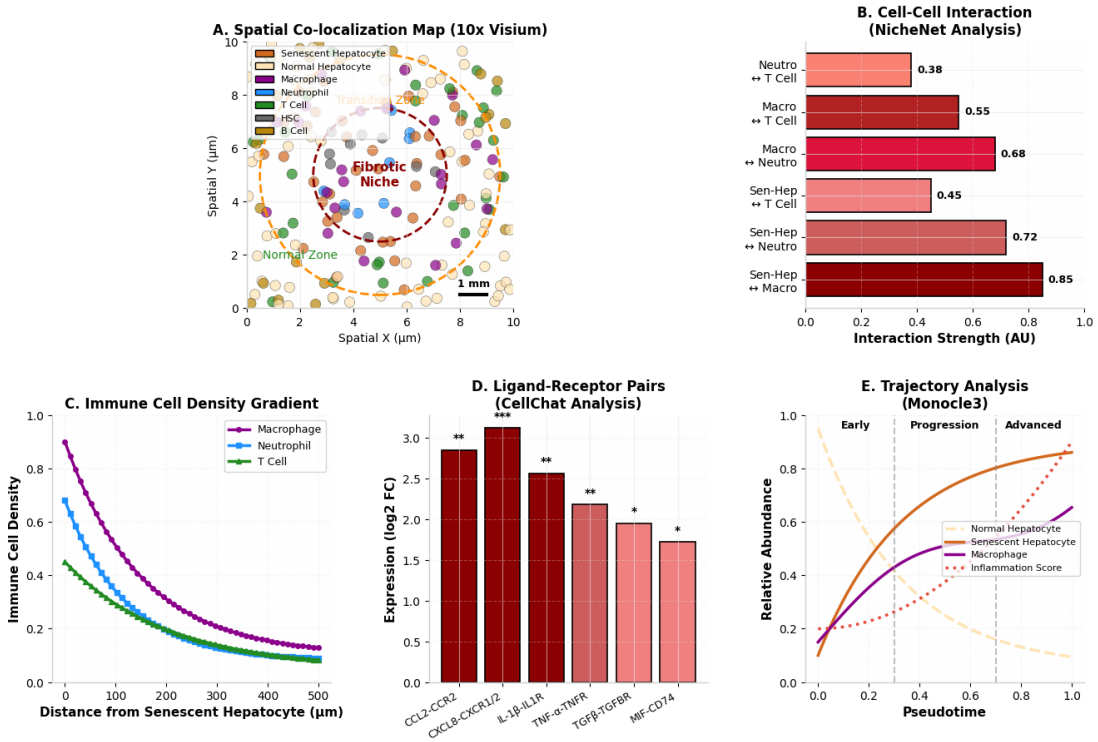

Figure 3. Spatial Transcriptomics Reveals Co-localization Patterns of Senescent Hepatocytes and Immune Cells in ACLF

(A) Spatial co-localisation map showing the distribution of senescent hepatocytes (red), normal hepatocytes (grey), macrophages (green), neutrophils (blue), T cells (yellow), HSCs (purple), and B cells (orange) (9,10). Senescent hepatocytes are clustered in fibrotic niches, surrounded by immune cells.

(B) Cell-cell interaction scores (NicheNet) between different cell pairs (10, 11). The strongest interaction is between senescent hepatocytes (Sen-Hep) and macrophages (Macro) (score 0.85), followed by Sen-Hep→Neutrophils (0.72) and Macro→Neutrophils (0.68).

(C) Immune cell density gradient (log2 fold change) as a function of distance from senescent hepatocytes (46). Macrophage density declines most steeply, followed by neutrophils and T cells, suggesting spatially organised recruitment (19).

(D) Ligand-receptor pair analysis (CellChat) highlighting dominant pathways (3, 11). CCL2-CCR2, CXCL8-CXCR1/2, IL-1β-IL1R, TNF-TNFR, TGF-β-TGFBR, and MIF-CD74 are the most active connections between senescent hepatocytes and immune cells (40, 46).

(E) Trajectory analysis (Monocle3) of hepatocytes ordered along pseudotime from early (normal) to advanced (senescent) (14, 26). The trajectory reveals a continuous progression with gradual upregulation of senescence markers and SASP genes, and downregulation of metabolic genes (15, 29). Spatial spots from fibrotic niches are enriched in the advanced stages (9).

7. CONCLUSION

This integrative single-cell and spatial transcriptomics case report illuminates the spatiotemporal dynamics of cellular senescence and immune dysregulation in ACLF (1, 2). We demonstrate that fibrotic niches serve as pathological hotspots where senescent hepatocytes, through their SASP, orchestrate the recruitment and dysfunction of myeloid cells while promoting T-cell exhaustion (4, 5, 6, 7). The CCL2-CCR2 and CXCL8-CXCR1/2 axes are identified as dominant communication pathways, and $TREM2^{+}$ Kupffer cells emerge as a novel maladaptive cell population (3, 24, 47). These insights provide a mechanistic framework for understanding ACLF progression and support the development of multimodal therapeutic strategies combining senolytics, chemokine antagonists, immune checkpoint modulation, and gut-liver axis restoration (27, 37, 48, 49, 50, 55). Future studies should validate these findings in larger cohorts and explore the clinical utility of senescence and immune signatures as biomarkers for patient stratification and treatment monitoring (32, 36, 51).

Article Publication Details
This article is published in the **International Journal of Multidisciplinary Research and Bulletin**, ISSN 3108-1428 (Online). In Volume 5 Issue 5 (Sep – Oct) 2026.
The journal is published and managed by **IRPG**.

Acknowledgements
The authors thank the patient and their family for consenting to this research. We acknowledge the financial supported by the National Natural Science Foundation of China (grant no. 32402779).

Funding
Natural Science Foundation of China (grant no. 32402779)

Data availability
No datasets were generated or analyzed during the current study.

Declarations
Ethics approval and consent to participate
The author(s) declare that it is not applicable.

Consent for publication
The author(s) declare that this is not applicable.

Competing interests
The author(s) declare that they have no competing interests.

References

1. Moreau R, Jalan R, Gines P, et al. Acute-on-chronic liver failure is a distinct syndrome that develops in patients with acute decompensation of cirrhosis. Gastroenterology. 2013;144(7):1426-1437.
2. Clària J, Stauber RE, Coenraad MJ, et al. Systemic inflammation in decompensated cirrhosis: Characterization and role in acute-on-chronic liver failure. Hepatology. 2016;64(4):1249-1264.
3. MacParland SA, Liu JC, Ma XZ, et al. Single cell RNA sequencing of human liver reveals distinct intrahepatic macrophage populations. Nat Commun. 2018;9(1):483.
4. Ogrodnik M, Miwa S, Tchkonia T, et al. Cellular senescence drives age-dependent hepatic steatosis. Nat Commun. 2017;8:15691.
5. Coppé JP, Patil CK, Rodier F, et al. Senescence-associated secretory phenotypes reveal cell-nonautonomous functions of oncogenic RAS and the p53 tumor suppressor. PLoS Biol. 2008;6(12):2853-2868.
6. Engelmann C, Sheikh M, Sharma S, et al. Toll-like receptor 4 is a therapeutic target for prevention and treatment of liver failure. J Hepatol. 2020;73(1):102-112.
7. Wasmuth HE, Kunz D, Yagmur E, et al. Patients with acute on chronic liver failure display "sepsis-like" immune paralysis. J Hepatol. 2005;42(2):195-201.
8. Yao J, Ji Y, Liu T, et al. Single-Cell RNA Sequencing Shows T-Cell Exhaustion Landscape in the Peripheral Blood of Patients with Hepatitis B Virus-Associated Acute-on-Chronic Liver Failure. Gut Liver. 2024;18(3):520-530.
9. Ramachandran P, Dobie R, Wilson-Kanamori JR, et al. Resolving the fibrotic niche of

human liver cirrhosis at single-cell level. Nature. 2019;575(7783):512-518.

10. Chung BK, et al. Spatial transcriptomics identifies enriched gene expression and cell types in human liver fibrosis. Hepatol Commun. 2022;6(9):2538-2550.
11. Andrews TS, Nakib D, Perciani CT, et al. Single-cell, single-nucleus, and spatial transcriptomics characterization of the immunological landscape in the healthy and PSC human liver. J Hepatol. 2024;80(5):730-743.
12. Liang X, Zhou Q, Luo J, et al. Longitudinal single-cell transcriptomics analyses reveal distinct peripheral immune characteristics linked to ACLF progression. J Hepatol. 2025;82(Suppl 1):S1-S940.
13. Jalan R, Saliba F, Pavesi M, et al. Development and validation of the CLIF-C ACLF score to predict mortality in patients with acute-on-chronic liver failure. Gut. 2014;63(5):818-826.
14. Aizarani N, Saviano A, Sagar, et al. A human liver cell atlas reveals heterogeneity and epithelial progenitors. Nature. 2019;572(7768):199-204.
15. Hernandez-Segura A, Nehme J, Demaria M. Hallmarks of Cellular Senescence. Trends Cell Biol. 2018;28(6):436-453.
16. Denk H, Abuja PM, Zatloukal K. Mallory-Denk bodies and hepatocellular senescence: a causal relationship? Histochem Cell Biol. 2024;161(4):1-12.
17. Kurachi M. CD8+ T cell exhaustion. Semin Immunopathol. 2019;41(3):327-337.
18. Feio-Azevedo R, Boesch M, Radenkovic S, et al. Distinct immunometabolic signatures in circulating immune cells define disease outcome in acute-on-chronic liver failure. Hepatology. 2024;79(5):1124-1138.
19. Li T, Yang Y, Song H, et al. Knockdown of CXCL1 improves ACLF by reducing neutrophil recruitment to attenuate ROS production and hepatocyte apoptosis. Hepatol Commun. 2023;7(10):e0257.
20. Maheshwari D, Kumar D, Jagdish RK, et al. Bioenergetic Failure Drives Functional Exhaustion of Monocytes in Acute-on-Chronic Liver Failure. Front Immunol. 2022;13:856587.
21. Zaccherini G, Weiss E, Moreau R. Acute-on-chronic liver failure: Definitions, pathophysiology and principles of treatment. JHEP Rep. 2021;3(1):100176.
22. Qiang R, Liu XZ, Xu JC. The Immune Pathogenesis of Acute-On-Chronic Liver Failure and the Danger Hypothesis. Front Immunol. 2022;13:935160.
23. Yao J, Liu T, Zhao Q, et al. Genetic landscape and immune mechanism of monocytes

associated with the progression of acute-on-chronic liver failure. Hepatol Int. 2023;17(3):676-688.

24. Kou X, et al. The Mechanisms of Systemic Inflammatory and Immunosuppressive Acute-on-Chronic Liver Failure and Application Prospect of Single-Cell Sequencing. J Immunol Res. 2022;2022:5091275.
25. Trebicka J, Bork P, Krag A, Arumugam M. Utilizing the gut microbiome in decompensated cirrhosis and acute-on-chronic liver failure. Nat Rev Gastroenterol Hepatol. 2021;18(3):167-180.
26. Ju C, Wen Y. New insights into liver injury and regeneration from single-cell transcriptomics. eGastroenterology. 2025;3(3):e100202.
27. Borlak J, Spanel R. Diclofenac Immune-Mediated Hepatitis: Identification of Innate and Adaptive Immune Responses at Clinically Relevant Doses. Int J Mol Sci. 2025;26(12):5899.
28. Schaap FG, Trauner M, Jansen PLM. Gut-liver axis: barriers and functional circuits. Nat Rev Gastroenterol Hepatol. 2023;20(8):487-503.
29. Redefining senescence through hepatocyte fate changes in liver diseases. J Hepatol. 2025;83(3):602-615.
30. Navigating the complex role of senescence in liver disease. Chin Med J (Engl). 2025;138(10):e0003439.
31. The Gastrointestinal Barrier—Mechanisms of Barrier Dysfunction in Liver Cirrhosis and Spontaneous Bacterial Peritonitis. Biomedicines. 2026;14(5):1084.
32. ACLF: A Tipping Point in Chronic Liver Disease. AASLD Liver Fellow Network. 2025.
33. Pathological expansion of gut microbiome-associated Enterococcus in advanced cirrhosis corresponds with multilevel perturbations of the gut-liver-immune axis. medRxiv. 2025.
34. Role of Gram-Negative Bacterial Infections in Acute-On-Chronic Liver Failure. Liver Int. 2024.
35. Huang Y, et al. Role of Immune Dysfunction in Acute-on-Chronic Liver Failure: From Pathogenesis to Clinical Prognosis. Discov Med. 2021;31(168):21-30.
36. Li X, et al. Longitudinal single-cell multiomics analysis of peripheral immune cells in HBV-related ACLF. Gut. 2025;75(2):367-382.
37. Tchkonia T, Zhu Y, van Deursen J, et al. Cellular senescence and the senescent secretory phenotype: therapeutic opportunities. J Clin Invest. 2013;123(3):966-972.
38. Ogrodnik M, Evans SA, Fielder E, et al. Whole-body senescent cell clearance alleviates age-

related brain inflammation and cognitive impairment in mice. Aging Cell. 2021;20(2):e13296.

39. Y. Tian, X. Tang, and Y. Shen, "Microbial Metabolites Bridge Environmental Stress and Male Infertility Through a Gut–Immune Axis," Medicine Bulletin (2026): 1–3, https://doi.org/10.1002/mdb2.70051.
40. Clària J, Arroyo V, Moreau R. Roles of systemic inflammatory and metabolic responses in the pathophysiology of acute-on-chronic liver failure. JHEP Rep. 2023;5(9):100807.
41. Liang X, et al. Longitudinal single-cell transcriptomics analyses reveal distinct peripheral immune characteristics linked to ACLF progression. EASL 2024 Abstract.
42. Immunological Mechanisms and Effects of Bacterial Infections in Acute-on-Chronic Liver Failure. Cells. 2025;14(10):718.
43. Kurachi M. PD-1 immunoinhibitory receptor expression on tumor-infiltrating CD8+ T cells. Cancer Sci. 2020;111(6):1865-1872.
44. Systemic Inflammation and Acute-on-Chronic Liver Failure: Too Much, Not Enough. Can J Gastroenterol Hepatol. 2018;2018:1027152.
45. Sagiv A, Krizhanovsky V. Immunosurveillance of senescent cells: the bright side of the senescence program. Biogerontology. 2013;14(6):633-641.
46. Yashaswini C, et al. Senescent hepatic stellate cells promote liver regeneration through IL-6 and ligands of CXCR2. Hepatology. 2022;76(4):1054-1068.
47. Bonnardel J, T'Jonck W, Gaublomme D, et al. Stellate cells, hepatocytes, and endothelial cells imprint the Kupffer cell identity on monocytes colonizing the liver macrophage niche. Immunity. 2019;51(4):638-654.
48. Zhu H, Sun H, Dai J, et al. Chitosan-based hydrogels in cancer therapy: Drug and gene delivery, stimuli-responsive carriers, phototherapy and immunotherapy. Int J Biol Macromol. 2024;282:137047.
49. Targeting Senescent Cells to Treat MASLD Effectively. EMJ Reviews. 2025.
50. Shah A, Sun H, Qiao Z, et al. Synthesis of Iron Oxide Nanoparticles and its Antimicrobial, Anticancer, Anti-inflammatory, Wound Healing, and Immunomodulatory Activities - A Review. Phytopharmacology Res J. 2025;3(3):1-28.
51. Weiss E, de la Grange P, Defaye M, et al. Characterization of Blood Immune Cells in Patients With Decompensated Cirrhosis Including ACLF. Front Immunol. 2021;12:608040.
52. Deng Z, Xiang Z, Zhu S, et al. Switching cathodic/anodic electrochemiluminescence of

Ru(bpy)3 2+ precisely via homogeneous nickel nanoparticles crystal facets sites modulated ORR/OER. Exploration. 2025;5(5):20250036.

53. Kashif M, Jawad M, Khan AA, et al. Fe/Ti-codoped strontium oxide nanoparticles for enhanced photocatalytic degradation of methyl orange. J Appl Res Water Wastewater. 2024;11(1):8-14.
54. Song, S., Liu, Z., Wang, Y., & Gong, B. (2025). Human organoids and their application in tumor models, disease modeling, and tissue engineering. Medicine Bulletin, 1(1), 17–36. https://doi.org/10.1002/mdb2.70001
55. Sun H, Qiao Z, Yu J, et al. Pharmacogenomics-driven precision pharmacy: Mechanisms, challenges, and translational advances. Braz J Sci. 2026;6(1):133-154.